



Heterogeneous & Homogeneous & Bio- & Nano-

CHEM **CAT** CHEM

CATALYSIS

Accepted Article

Title: Hollow NiCo Layered Double Hydroxide Supported Pd Catalysts for Superior Hydrogen Evolution Activity for Hydrolysis of Ammonia Borane

Authors: Yinghua Zhou, Suqin Wang, Zhiyan Zhang, Nicholas Williams, Yong Cheng, and Jing Gu

This manuscript has been accepted after peer review and appears as an Accepted Article online prior to editing, proofing, and formal publication of the final Version of Record (VoR). This work is currently citable by using the Digital Object Identifier (DOI) given below. The VoR will be published online in Early View as soon as possible and may be different to this Accepted Article as a result of editing. Readers should obtain the VoR from the journal website shown below when it is published to ensure accuracy of information. The authors are responsible for the content of this Accepted Article.

To be cited as: *ChemCatChem* 10.1002/cctc.201800459

Link to VoR: <http://dx.doi.org/10.1002/cctc.201800459>

WILEY-VCH

www.chemcatchem.org



COMMUNICATION

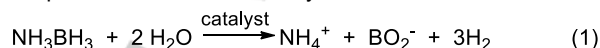
Hollow NiCo Layered Double Hydroxide Supported Pd Catalysts for Superior Hydrogen Evolution Activity for Hydrolysis of Ammonia Borane

Ying-Hua Zhou,^{*,[a, b]} Suqin Wang,^[a] Zhiyan Zhang,^[a] Nicholas Williams,^[b] Yong Cheng,^[a] and Jing Gu^{*,[b]}

Abstract: Although ammonia borane (NH₃BH₃, AB) has been identified as an excellent hydrogen storage medium, there is still a great challenge towards developing a highly active catalyst that can function at mild conditions for controllable hydrogen release. The synergistic effect induced by the interactions between metal nanoparticles and a support has been widely applied in the thermo-catalytic conversion process. In this work, Pd nanoparticles (NPs) highly dispersed onto hollow NiCo layered double hydroxide (LDH), were designed for efficient hydrogen generation from AB at room temperature. During the hydrolytic dehydrogenation of AB, Pd/α-LDH and Pd/β-LDH had been demonstrated to exhibit catalytic activities with a total turnover frequency (TOF) of 49.5 and 28.1 min⁻¹ and an activation energy (E_a) of 20.56 and 37.56 kJ mol⁻¹, respectively at 298 K, outperforming most Pd-based catalysts. The improved catalytic effect can be contributed to the controllable size, fine distribution of Pd NPs, and the collaborative effect provided by the hydroxide of α-LDH with intercalated anions(OH⁻). This catalysts design principle can be easily transferred into other catalyst research fields for energy conversion and storage purposes.

Hydrogen is the simplest and cleanest fuel carrier, usually utilized in a fuel cell setup to generate power, producing only water and heat as byproducts.^[1,2] Hydrogen produces the highest energy per mass among any fuel. Unfortunately, due to its low volumetric density under ambient conditions, the major obstacle that prevents the building of the hydrogen economy is the development of advanced storage methodology that have potential for higher energy density per volume.^[3-5] Subsequently, it is also important for the development of technologies that could release of hydrogen in a controllable fashion under mild conditions from said medium. The chemical hydrides are promising candidates due to their high gravimetric hydrogen densities, favorable thermodynamic, and kinetic properties

towards dehydrogenation.^[6,7] Among them, ammonia borane (NH₃BH₃, AB) is considered to be an efficient carrier, with superb stability in aqueous and methanol solutions, a high volumetric density of 146 g·L⁻¹, and a hydrogen capacity of 196 g·kg⁻¹.^[8,9] Hydrogen stored in the AB can be released by either thermal decomposition or solvolysis.^[10,11] Considering the high energy input of thermal decomposition (> 100 °C), numerous research has been focused on the hydrolytic dehydrogenation of AB (eq 1) in the presence of metal catalysts under ambient conditions.^[12]



Hundreds of metal catalysts have been exploited to promote the efficiency of AB dehydrogenation.^[13] Among them, Pd NPs based catalytic systems served as a favorable catalyst for AB hydrolysis, due to their lower costs relative to other precious metals and higher activity compared to the non-noble metal catalysts.^[14,15] It is well known that although the small-sized metal NPs can provide more catalytic active sites, such NPs usually suffer from deactivation and instability issues induced by the migration and agglomeration of metal NPs in the reaction. This problem can usually be solved by immobilizing NPs on the appropriate catalyst supports.^[16]

Layered double hydroxides (LDH) are a class of synthetic anionic clays, which frequently act as a support for catalysts. LDH can be represented by a formula of [M²⁺_{1-x} M³⁺_x(OH)₂]^{x+} (Aⁿ⁻)_{x/n} · mH₂O, which features the positive-charged brucite Mg(OH)₂-like host layers (M²⁺ and M³⁺ represent metallic cations) and exchangeable interlayer galleries, consisting of anions (Aⁿ⁻) and water (H₂O).^[17] Metal catalysts tethered onto LDH experience improved catalytic performance by enhancing catalytic efficiency, selectivity and stability. The metal NPs can be placed in a controllable and highly dispersed manner on the plane of LDH, while the preferred orientation of anions will be located at the interlayer.^[18] The LDH selected here is a NiCo compound, and was chosen for three reasons: 1) this LDH had been proven to act as an excellent electroactive material, which may facilitate the charge transfer in between the metal and the support.^[19] 2) A metal organic framework (MOF) template can be used to as a simple precursor to construct these LDH nanocomposites. After conversion, it forms a hollow cubic structure, which will increase the surface-to-volume ratios enhancing the support of the catalysts.^[20] 3) Among NiCo LDH compounds studied, α-phase has already received extensive attentions,^[21] whereas the β-phase, which might be another active phase, had been rarely investigated. The α-structure of LDH consists of Ni(OH)₂ layers with intercalated anions or water. However, the β-form presents a hexagonal close-packed structure of Ni²⁺ and OH⁻ ions.^[22] In addition to its support functional role, we suspected the OH⁻ anion on LDH could further improve the catalytic activity of the metal

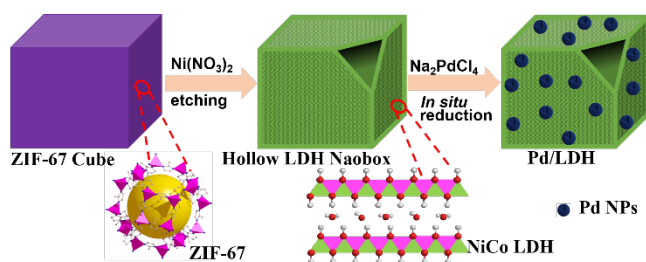
[a] Associate Prof. Y.-H. Zhou, S. Wang, Z. Zhang
The Key Laboratory of Functional Molecular Solids, Ministry of Education, Anhui Laboratory of Molecule-Based Materials (State Key Laboratory Cultivation Base),
College of Chemistry and Materials Science
Anhui Normal University
Wuhu, Anhui 241002, China
E-mail: yhzhou@ahnu.edu.cn

[b] Assistant Prof. J. Gu
Department of Chemistry and Biochemistry
San Diego State University
San Diego, CA 92182-1030, USA
E-mail: jgu@sdsu.edu

Supporting information for this article is given via a link at the end of the document.

COMMUNICATION

decorated LDH based on the following discoveries. Recently, the catalytic mechanism of AB originated hydrogen releasing has been studied, in which it demonstrated that the formation of hydroxyl group from the deprotonation of water molecule is the rate-determining step.^[23] Furthermore, it is shown that the OH⁻ anion could significantly promote the catalytic activity during the controlled-release of hydrogen from AB.^[24] Therefore, it is highly desirable to develop a catalyst with the superior efficiency of AB hydrolysis by the synergistic effects induced by both the interactions between metal NPs and the natural hydroxyl anions on LDHs.



Scheme 1. Schematic diagram for the preparation of Pd/LDH.

Herein, we report a rational design and fabrication strategy of a nanocatalyst with highly dispersed Pd NPs anchored to the NiCo LDH hollow nanoboxes. The NiCo LDH nanoboxes were synthesized by the acidic etching of ZIF-67 nanocubes. The loading of Pd NPs onto NiCo LDH nanocubes was achieved by *in situ* reduction of Pd NPs via NiCo LDH, occurring after the electrostatic attraction between PdCl₄²⁻ and positively-charged LDH in solution. NiCo LDH would serve as both the reductant and as a size-controlling support (Scheme 1). In comparison with Pd/β-LDH, Pd/α-LDH catalyst exhibited the superior catalytic activity and durability towards the AB hydrolysis with a TOF value of 49.5 mol_{H₂} mol_{Pd}⁻¹ min⁻¹ and E_a value of 20.56 kJ mol⁻¹ under ambient conditions.

ZIF-67 nanocubes were obtained by a simple precipitation reaction, in which Co(NO₃)₂ was added into an aqueous solution of 2-methylimidazole at room temperature.^[25] The as-synthesized ZIF-67 structure was confirmed by powder X-ray diffraction (XRD) (Figure S1), in which the diffraction peaks of as-synthesized ZIF-67 matches well with the simulated results.^[26] When ZIF-67 nanocubes, a sacrificial template, were reacted with Ni(NO₃)₂ in an ethanol solution, the diffraction peaks of ZIF-67 disappeared, indicating the complete conversion of ZIF-67 into the formation of NiCo LDH during the acidic etching process. The FESEM and TEM images of ZIF-67 and the converted NiCo LDH are shown in Figure 1, indicating that the original ZIF-67 nanocubes assemble with a highly uniform size of ~300 nm (Figure 1a and 1b). Since the inside of LDH nanocubes are empty, the faces of nanoboxes might collapse and form a fake hole as demonstrated in the SEM image (Figure 1c). However, TEM (Figure 1d) imaging unambiguously reveals that the surface of the nanoboxes were completely enclosed by LDH nanosheets. More LDH nanosheets are present on the edges of the walls than on the center of the nanoboxes faces (Figure S2a). Furthermore, TEM (Figure 1d) image reveals a hollow interior presented at the center of the nanocubes by the obvious image contrast difference in between

the edge and center. At the same time, NiCo LDH TEM imaging (Figure S3) taken from a direction in between two faces demonstrated that all faces of the nanobox are closed. The thickness of the shell is about 50 nm, while the depth of the hollow box is ca. 200 nm. The elemental mapping of a LDH (Figure S2) nanobox confirms the uniform distribution of the Ni, Co and O elements throughout the surface of the nanobox. The formation process of hollow LDH nanoboxes might be explained as the following process: firstly, during the reaction between Ni(NO₃)₂ and ZIF-67, an extra proton will be produced. The generated proton will etch away the center of the ZIF-67 nanocubes while the Ni²⁺ ions hydrolyze. The Co²⁺ ions released from the decomposed ZIF-67 may be partially oxidized by NO₃⁻ ions or O₂ in the solution to form Co³⁺.^[27] As the reaction progresses, the Co²⁺/Co³⁺ ions will co-precipitate with Ni²⁺ ions to form a layer of NiCo LDH, which eventually leads to formation of hollow NiCo LDH nanoboxes.

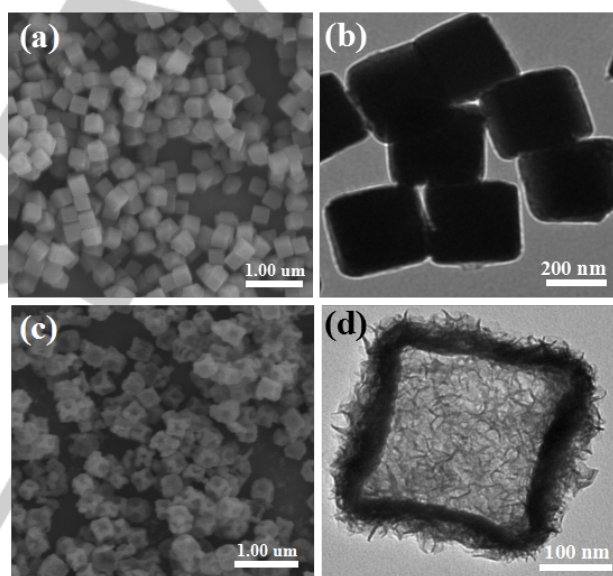


Figure 1. SEM(left) and TEM(right) images of ZIF-67 nanocubes (a, b) and NiCo LDH nanoboxes (c, d).

TEM images (Figure 2a, b) of the 0.0025 mol/g Pd/α-LDH indicate that the Pd NPs uniformly dispersed on the surface of the LDH nanoboxes, showing hollow nanobox morphology with a size of ~200 nm × 200 nm. The size distribution of Pd NPs was determined to be in ranges from 3.5-7.5 nm with an average particle size of ca. 5.6 nm (Figure 2c). HRTEM imaging of the 0.0025mol/g Pd/α-LDH indicates that the lattice space of the Pd NPs is 0.227 nm (Figure 2d), corresponding well with the lattice spacing of Pd(111) (JCPDS no. 46-1043). The selected area diffraction (SAED) pattern inset in Figure 2d further proves the crystalline structure of Pd nanoparticle. X-ray energy dispersive spectroscopy (EDS) (Figure S4) demonstrates the co-existence of cobalt, nickel and palladium elements in the catalyst. The palladium atomic ratio in Pd/α-LDH and Pd/β-LDH were found to be 23.78 wt.% and 21.38 wt.%, respectively by ICP-OES (Table S1). Furthermore, TEM were utilized here to characterize the

COMMUNICATION

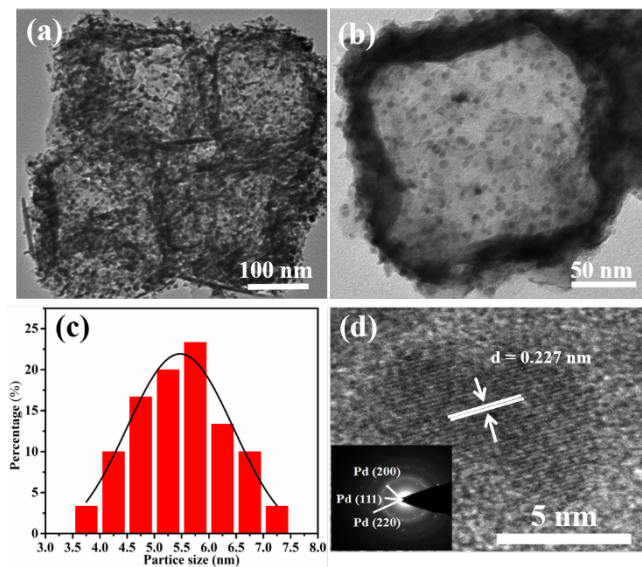


Figure 2. Representative TEM images (a, b), the corresponding distribution size histograms (c) and HRTEM image (d) of 0.0025 mol/g Pd/α-LDH. Inset in (d) is the SAED pattern recorded from the whole particle.

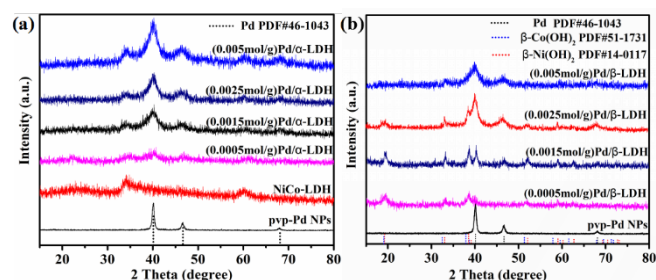


Figure 3. The XRD patterns of Pd/α-LDH (a) and Pd/β-LDH (b) with various Pd NPs loading quantities.

structures and compositions of NiCo LDH immobilized different loading amounts of Pd NPs (0.0005, 0.0015, 0.0025, 0.005 mol/g Pd/α-LDH and Pd/β-LDH) (Figure S5 and S6). From the TEM images, an intensive degree of particle aggregation and degradation of the original hollow LDH nanoboxes was noticed with a Pd high loading amount of 0.005 mol/g Pd/α-LDH and Pd/β-LDH. One possible reason is that hollow LDH nanoboxes lack sufficient strength to withstand a large number of nanoparticles resting on its surfaces, resulting in the collapse of the structure. Otherwise, the size and shape of the metal NPs does not show obvious change with the tuning of loading amounts. However, the density of NPs on the LDHs layer increases with the increasing loading concentration. Due to the structure confinement effect induced by the nanoporous LDHs, the Pd NPs are highly dispersed and have a well-proportioned size distribution. As compared with α-phase NiCo LDH (Figure 2), a similar particle size and dispersity were observed for the β phase Pd/β-LDH (Figure S6). Also, the chemical structure information of pure Pd, NiCo LDH and Pd/LDH were studied by the XRD (Figure 3). XRD patterns of the samples exhibit characteristic reflections of Pd

metal, as well as the peaks of NiCo LDH. Three peaks located at 40.1, 46.7 and 68.1°, corresponding to the crystal structure of Pd (JCPDS no. 46-1043) at (111), (200), (220) orientations were identified. Another three characteristic peaks, corresponding to (006), (009), and (110) phases of a typical NiCo LDH structure, can be observed at 22.5, 33.7, and 60.2° (Figure 3a), respectively.^[24] In respect to the XRD patterns of Pd/β-LDH (Figure 3b), exclusive peaks can be identified at 19.2, 33.0, 38.5, 52.1, 59.0, and 62.7°, which correspond to the (001), (110), (101), (102), (110), (111) facets of β-phase Ni(OH)₂ (JCPDS no. 14-0117)^[28] and Co(OH)₂ (JCPDS no. 51-1731).

XPS was employed here to further uncover the chemical nature of the catalysts. Figure 4 shows the XPS survey spectra of the Pd/α-LDH, indicating the presence of Pd, Ni, Co, and O. The binding energies (BEs) of the 335.3 and 340.5 eV located in the Pd 3d_{5/2} and 3d_{3/2} range can be ascribed to presence of the metallic Pd(0) state (Figure 4a). Unexpectedly, the Pd²⁺ peaks with BE of 337.0 and 342.4 eV are also observed (Figure 4b). The Pd²⁺ might have originated from two sources: 1. It might be generated from the precursor Na₂PdCl₄. However, the 3d_{5/2} peak of Pd²⁺ in the Na₂PdCl₄ should be located at 338.0 eV. Thus, the possibility

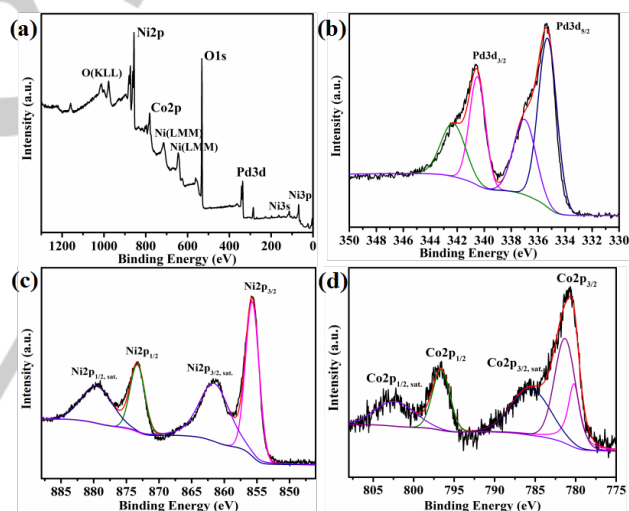


Figure 4. The XPS Survey spectra of Pd/α-LDH sample (a), the Pd 3d peak (b), Ni 2p peak (c), and Co 2p peak (d) of the Pd/α-LDH sample.

of the PdCl₄²⁻ absorbed on LDH sheet is excluded. 2. The Pd²⁺ peaks might be assigned to PdO at the surface of Pd NPs due to the exposure of oxygen, which has been observed from previous research.^[29] The Ni 2p spectrum reveals two satellite peaks (BE = 861.7 and 880 eV) and two main peaks (BE= 855.7 and 873.7 eV) (Figure 4c), which are separately identified as Ni 2p_{3/2} and Ni 2p_{1/2} verifying the existence of Ni²⁺. For the Co 2p spectrum, the Co²⁺ peaks were located at 781.3 and 796.6 eV with two accompanied satellite peaks (BE=785.8 and 802.4 eV) (Figure 4d). Moreover, the peaks presents at the 780.1 eV are attributed to the generation of Co³⁺ from Co²⁺.^[30] The formation of Co³⁺ is an indication that the well-controlled size of Pd NPs was established by the redox reactions happening in between Co²⁺ in the NiCo

COMMUNICATION

LDH support and PdCl_4^{2-} in the solution,^[31] considering that the potential value of $\varphi(\text{PdCl}_4^{2-}/\text{Pd})^\theta$ and $\varphi(\text{Co}(\text{OH})_3/\text{Co}(\text{OH})_2)^\theta$ is 0.591 and 0.17 V vs SHE, respectively.

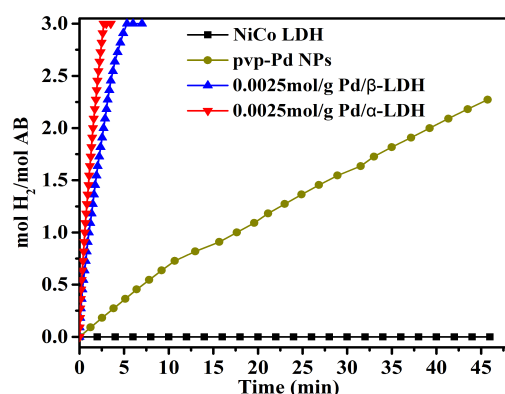


Figure 5. Time course for hydrogen production from AB aqueous solution (5 mL, 0.2 M) over pvp-Pd NPs, NiCo LDH, Pd/α-LDH and Pd/β-LDH at 298 K.

The catalysts activity was investigated by hydrolyzing of AB, for hydrogen generation, at room temperature. Pure NiCo LDH is nearly inactive, whereas PVP-protected Pd NPs release 2.3 equiv H_2 per AB in about 46 min (Figure 5). The catalytic activities for 0.0025 mol/g Pd/α-LDH and Pd/β-LDH enhanced, with ~3 equiv H_2 per AB generated within only 2.80 min and 5.20 min, respectively. Moreover, based on Pd atom amounts determined by ICP-OES, the turnover frequency (TOF) of Pd/α-LDH has been found to be 49.5 min^{-1} , which is considerably better than that of Pd/β-LDH (28.1 min^{-1}). Table 1 displays the activities of 0.0025 mol/g Pd/α-LDH and Pd/β-LDH, in comparison with various Pd related catalysts documented in the literatures.^[14,15,32-39] Comparing with the other Pd catalysts, we conclude the Pd/α-LDH presented in this study is one of the state-of-art Pd catalysts for AB hydrolysis. Mechanistically, the outstanding performance of this Pd catalyst can be explained by the synergic effect of the controlled size and distribution loading of the Pd catalyst with the presence of interlayer anion (OH^-), all of which improved the kinetics of the hydrolysis process. As demonstrated by He *et al.* using kinetic isotope effect measurements, breaking the O-H bond in the metal-activated H_2O is the rate determining step in the reaction of AB hydrolysis catalyzed by metal NPs.^[23] The introduction of OH^- during AB hydrolysis should promote the kinetics of hydrolysis intermediate and facilitate the hydrolytic H_2 evolution process in the confined nanostructure medium. Both phases contain OH^- anions, which is expected to improve the catalytic activity. Catalytically, the α-phases had superior performance compared to the β-phases. Better OH^- mobility in the α-phases than the β-phases could explain this phenomena.^[24] To verify this hypothesis, AB dehydrogenation over 0.0025 mol/g Pd/α-LDH had been performed with the different pH values. It was found that the catalytic rate of hydrogen production decreased (Figure S7) when the solution was adjusted to a pH value of 6 compared with pH 8. At the same time the rate of H_2 generation slightly increased when the pH value was raised from 8 to 12. However, the reaction rate dropped in a more alkaline medium

(pH 14), due to concentration of OH^- exceeding its optimum level.^[40] Pure LDH without loading Pd nanoparticles exhibits negligible catalytic activity, regardless of acidic or basic conditions. Therefore, it could be speculated that AB should be activated by metal NPs to produce the activated complex intermediates, which could be attacked by OH^- anions and/or water molecules in the following previously studied mechanistic steps.^[13,40,41]

Table 1. Catalytic activity of pallium-related catalysts in hydrogen generation from the hydrolysis of ammonia borane at 298K.

Catalyst	$\eta_{\text{metal}}/\eta_{\text{AB}}$	TOF (min^{-1})	E_a (kJ mol^{-1})	Ref.
Pd/α-LDH	0.022	49.5	20.56	This work
Pd/β-LDH	0.020	28.1	37.56	This work
Pd@MIL-101	0.0189	45	-	[14]
Pd/CeO ₂	0.011	29	68	[15]
RGO@Pd	0.06	26.3	40	[32]
Pd/PPy	0.002	21.1	33.5	[33]
Pd-CDG	0.005	15.5	-	[34]
Pd/graphene	0.056	9.7	30.82	[35]
Pd ₇₄ Co ₂₆ /MCN	0.027	208.1	58.8	[36]
Ag ₃ Pd ₂ /PDA-HNT	-	90	22.8	[37]
Pd@Co/graphene	0.09	37.5	-	[38]
Pd/PDA-Fe ₃ O ₄	0.00895	14.5	65	[39]

In optimizing the catalytic activity, the loading amount of Pd NPs immobilized to NiCo LDH is an influential parameter. As shown in figure S8 the catalytic activity is proportional to the amount of Pd NPs loaded (<0.0025 mol/g) if the structure remains intact. If the loading amount passes 0.0025 mol/g Pd/LDH, its activity will decrease. The possible reason is that the hollow structure of LDH nanoboxes cannot support catalysts on its surface after a certain loading amount, without collapsing, which is correlated well with the material characterization results (Figure S5 and S6).

Concurrently, temperature plays an important role in the process of hydrogen release from AB. The catalytic dehydrogenation rates of Pd/α-LDH and Pd/β-LDH towards AB hydrolysis at different temperatures were investigated (Figure 6). The results showed that the rate of hydrogen generation rate increased sharply when the temperature was increased from 298 to 318 K, indicating that a high reaction temperature will enhance dehydrogenation kinetics and release hydrogen at a slightly elevated temperature. According to the Arrhenius plots (Figures 6b, d),^[41,42] the obtained apparent activation energy (E_a) of the AB dehydrogenation involving Pd/α-LDH and Pd/β-LDH was calculated to be 20.56 and 37.56 kJ mol^{-1} , respectively. The E_a of Pd/α-LDH was lower than most other reported Pd metal catalysts. The ameliorable activity can be explained by the collaborative

COMMUNICATION

effects from the confined Pd nanoparticle and OH⁻ anion enhancing the hydrolysis kinetics.

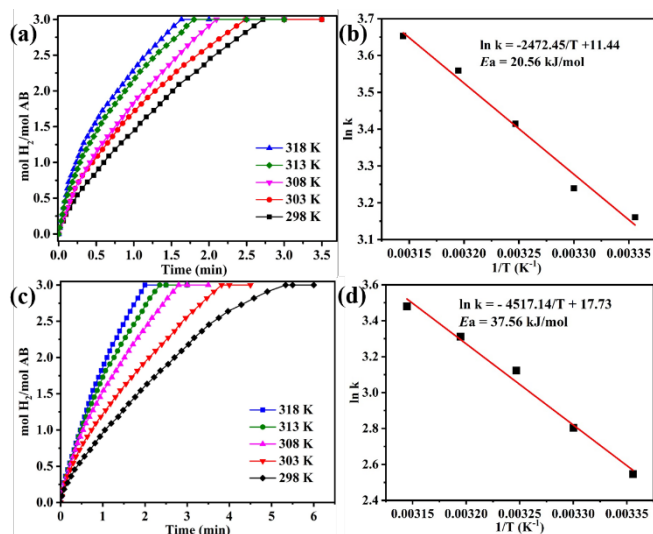


Figure 6. Time course for hydrogen production from AB aqueous solution (5 mL, 0.2 M) and Arrhenius plots of AB hydrolytic dehydrogenation catalyzed by Pd/α-LDH (a, b) and Pd/β-LDH (c, d) at different temperatures.

Moreover, the recyclable stability is another crucial parameter in the practical application of catalysts. The durability tests of Pd/α-LDH and Pd/β-LDH were carried out at 298 K. As shown in Figure 7, even after the 5 cycles, the productivity of H₂ remained almost unchanged. The reaction completion time of the dehydrogenation over Pd/α-LDH is 2.7, 3.5, 3.7, 3.9 and 4.5 min from first to fifth run, respectively. A slight decrease of reaction rate could be attributed to the increased concentration of BO₂⁻ product and the slight increase in the solution viscosity.^[43] After 5 cycles the integrity of Pd/α-LDH and Pd/β-LDH structures were almost entirely preserved and no aggregation of Pd was found to occur on the surface of LDH (Figure S9), indicating that the two supported NP catalysts had long durability, which can be attributed to the formation of NPs immobilized by hollow LDH supports.

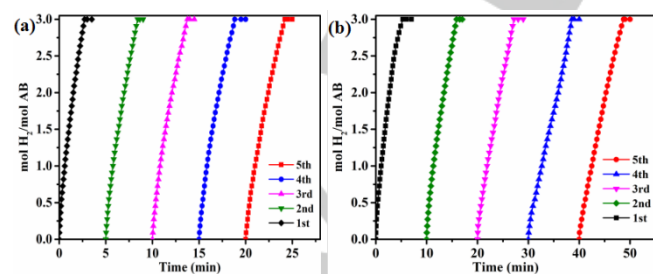


Figure 7. Durability test for hydrogen generated from AB aqueous solution over the as-synthesized catalysts at 298 K. Pd/α-LDH (a) and Pd/β-LDH (b).

In summary, hydrogen storage for subsequent use ranges from approaches utilizing high pressure, cryogenics, and high

temperature chemical compounds decomposition. A more efficient strategy for releasing hydrogen under ambient conditions facilitated by a suitable catalyst is critical for the economically feasible application of hydrogen storage. Herein, we designed a novel strategy to construct hollow NiCo LDH nanoboxes, which were employed as supports to immobilize highly active Pd NPs for AB hydrolysis. The NiCo LDH was directly converted from ZIF-67 nanocubes and changed into a hollow structure in the reaction process. The Pd/α-LDH exhibited superior catalytic activity with a TOF value of 49.5 min⁻¹ and an extremely low activation energy of 20.56 kJ mol⁻¹. The presence of interlayer anions (OH⁻) in the NiCo LDH played an important role of changing the binding kinetics and facilitating the activation process in the AB hydrolyses reaction. In addition, the as-synthesized catalysts exhibited high recycle stability. This work highlights that the rational design of materials with controllable morphologies as the catalysts supports can finely tune the interactions between supports and active metal NPs. This result demonstrated here could provide a great foundation in understanding the collaborative effects happening in between catalysts and the support materials for AB hydrolysis or other catalysts-support interaction in sustainable energy production and chemical synthesis applications.

Experimental Section

Materials. Cetrimonium bromide (CTAB, Aladdin), Cobalt nitrate (Co(NO₃)₂·6H₂O, Sinopharm Chemical Reagent), Nickel nitrate (Ni(NO₃)₂·6H₂O, Sinopharm Chemical Reagent), Palladium chloride (PdCl₂, Aldrich), Sodium chloride (NaCl, Sinopharm Chemical Reagent), Sodium hydroxide (NaOH, Sinopharm Chemical Reagent), ethanol (CH₃CH₂OH, Sinopharm Chemical Reagent, 99%) and ammonia borane (NH₃BH₃, Aldrich, 97%) were used as obtained. Deionized water was utilized in all experiments.

Synthesis of NiCo LDH nanoboxes: The ZIF-67 nanocubes were prepared *via* a simple surfactant-mediated method in an aqueous solution at the room temperature according to the previous literature.^[24] 30 mg of ZIF-67 nanocubes was dispersed into a round bottomed flask containing 20 mL ethanol and ultra-sonicated for 10 min. Further, the collected ZIF-67 nanocubes were reacted with Ni(NO₃)₂ to form NiCo LDH in an ethanol solution with minor modification compared to the literature.^[20] 5 mL of ethanol solution containing 100 mg of Ni(NO₃)₂·6H₂O was slowly added into the ethanol solution of ZIF-67. The mixture was refluxed for 1.5 h under stirring at 358 K. Finally, the product NiCo LDH, was collected by centrifugation, and subsequently washed with ethanol for three times and vacuum dried at 313 K for overnight.

Synthesis of Pd/α-LDH catalyst: Firstly, Na₂PdCl₄ stock solution was prepared by dissolving 44 mg of PdCl₂ and 29 mg of NaCl (2 equiv with respect to PdCl₂) in 25 mL of deionized water and stirred at 30 min. Secondly, 5 mL aqueous solution of 20 mg NiCo LDH was slowly added into 5 mL Na₂PdCl₄ solution under vigorous stirring. Thirdly, the pH value of solution was adjusted to ~10 by 0.1 M NaOH solution. After that, the mixture was hydrothermally treated at 373 K for 8 h to obtain Pd/α-LDH. The products were collected by filtration, washing with ethanol for three times and dried in vacuum at 313 K for 12 h.

Synthesis of Pd/β-LDH catalyst: The procedure was similar to the above except that condition of hydrothermal treatment is at an elevated temperature of 393 K for 6 h. Finally, the products were collected by

COMMUNICATION

washing with ethanol for three times and dried in vacuum at 313 K for 12 h.

Characterizations. The crystal phase properties of the synthesized nanocatalysts were analyzed with a Shimadzu X-ray diffractometer-6000 (XRD-6000) using Cu K α radiation at 40 kV and 40 mA ($\lambda = 0.1542$ nm). The morphologies and sizes of the samples were determined by using a transmission electron microscope (TEM, HT-7700), and energy dispersive X-ray (EDS) spectroscopy on Field Emission Scanning Electron Microscope (FESEM, S-4800) was used for elemental analysis. The lattice fringe was captured by a high-resolution transmission electron microscope (HRTEM, JEOL) at an accelerating voltage of 200 kV. X-ray photoelectron spectroscopy (XPS) measurements were performed with a Thermo Fisher Scientific ESCALAB 250X imaging electron spectrometer. Pd contents of the samples were determined by using Agilent 7700ce inductively coupled plasma-optical emission spectroscopy (ICP-OES) after the sample was completely dissolved in a mixture of aqua regia (HNO $_3$ /HCl = 1/3 volume ratio).

Catalytic hydrolytic dehydrogenation of AB: Generally, the hydrolytic dehydrogenation experiments are conducted in water at the given experimental temperature which were maintained by a circulating water bath. At the $t=0$ reaction time, the as-prepared catalyst (10.0 mg) was placed into 5 mL of deionized water with continuous stirring in a two-necked round-bottomed flask, and AB aqueous solution (1×10^{-3} mol, 5 mL) was quickly injected into the catalyst suspension. Out of the two necks, the first one is fitted with a gas outlet, and the other is sealed with a rubber cap. The neck is connected *via* the gas outlet to a water-filled gas burette. The volume of hydrogen gas generated was measured by recording the displacement of water level in the burette. The reaction was stopped when the water level stopped dropping. The catalytic activity of catalyst can be expressed with turnover frequency (TOF, min^{-1}). The corresponding calculating formula is as follow: $\text{TOF} = PV / (RT t n)$, where P is denoted as the standard atmospheric pressure (1.01×10^5 Pa); V is the total hydrogen volume which can be detected from the volume of drained water; R is a gas constant ($8.314 \text{ J K}^{-1} \text{ mol}^{-1}$); t is the consuming time; T (K) is the absolute temperature; and n is the total mols of Pd determined by ICP-OES.

Durability of catalysts: For the durability tests, after the hydrogen releasing was completed, another equal of AB solid was subsequently added to the above reaction system at room temperature. Such test cycles of the catalysts for hydrogen evolution from AB were repeated five times.

Procedure for the study of pH effects in the dehydrogenation of AB

Generally, the as-prepared catalyst (10.0 mg) is dissolved in 8 mL water with continuous stirring in a two-necked round-bottomed flask. NaOH or HCl dissolved in 1 mL water is then injected and used to adjust the pH of the solution, and the mixture is allowed to stir for 30 min. An aqueous solution of AB (1×10^{-3} mol, 1 mL) is injected in the catalyst suspension, and timing is started. The volume of hydrogen gas generated was measured by recording the displacement of water level in the burette. The reaction was stopped when the water level was not dropping.

Acknowledgements

This work was supported by the National Natural Science Foundation of China (NO. 21771004), Natural Science Foundation of Anhui Province (No. 1408085MKL21), Special and Excellent Research Fund of Anhui Normal University, Postgraduate Scientific Research and Innovation Project of Anhui

Normal University (No. 2015cxsj142), and Undergraduate Innovative training program of Anhui Normal University (201610370486, 201610370490). Jing Gu want to acknowledge the SDSU startup funds, the SDSU University Grants Program, and NSF award CEBT-1704992.

Keywords: ammonia borane • dehydrogenation • hydrolysis • heterogeneous catalysis • layered double hydroxide

- [1] A. C. Dillon, K. M. Jones, T. A. Bekkedahl, C. H. Kiang, D. S. Bethune, M. J. Heben, *Nature* **1997**, *386*, 377-379.
- [2] M. Z. Jacobson, W. G. Colella, D. M. Golden, *Science* **2005**, *308*, 1901-1905.
- [3] C. W. Hamilton, R. T. Baker, A. Staubitz, I. Manners, *Chem. Soc. Rev.* **2009**, *38*, 279-293.
- [4] L. J. Murray, M. Dinca, J. R. Long, *Chem. Soc. Rev.* **2009**, *38*, 1294-1314.
- [5] B. Sakintuna, F. Lamari-Darkrim, M. Hirscher, *Int. J. Hydrogen Energy* **2007**, *32*, 1121-1140.
- [6] A. F. Dalebrook, W. J. Gan, M. Grasmann, S. Moret, G. Laurenczy, *Chem. Commun.* **2013**, *49*, 8735-8751.
- [7] Z. Li, Q. Xu, *Acc. Chem. Res.* **2017**, *50*, 1449-1458.
- [8] H. L. Jiang, Q. Xu, *Catal. Today* **2011**, *170*, 56-63.
- [9] K. Aranishi, Q.-L. Zhu, Q. Xu, *ChemCatChem* **2014**, *6*, 1375-1379.
- [10] A. Staubitz, A. P. M. Robertson, I. Manners, *Chem. Rev.* **2010**, *110*, 4079-4124.
- [11] L. Cui, X. Cao, X. Sun, W. Yang, J. Liu, *ChemCatChem* **2018**, *10*, 710-715.
- [12] a) T. Karaca, M. Sevim, Ö. Metin, *ChemCatChem* **2017**, *9*, 4185-4190; b) Z. J. Liang, X. Z. Xiao, X. Y. Yu, X. Huang, Y. Q. Jiang, X. L. Fan, L. X. Chen, *J. Alloys Compd.* **2018**, *741*, 501-508.
- [13] a) W.-W. Zhan, Q.-L. Zhu, Q. Xu, *ACS Catal.* **2016**, *6*, 6892-6905; b) C. L. Xu, M. Hu, Q. Wang, G. Y. Fan, Y. Wang, Y. Zhang, D. J. Gao, J. Bi, *Dalton Trans.* **2018**, *47*, 2561-2567; c) J. Q. Chen, M. Hu, M. Ming, C. L. Xu, Y. Wang, Y. Zhang, J. T. Wu, D. J. Gao, J. Si, G. Y. Fan, *Int. J. Hydrogen Energy* **2018**, *43*, 2718-2725; d) C. Yu, X. F. Guo, M. Q. Shen, B. Shen, M. Muzzio, Z. Y. Yin, Q. Li, Z. Xi, J. R. Li, C. T. Seto, S. H. Sun, *Angew. Chem. Int. Ed.* **2018**, *57*, 451-455.
- [14] H. Dai, J. Su, K. Hu, W. Luo, G. Cheng, *Int. J. Hydrogen Energy* **2014**, *39*, 4947-4953.
- [15] Y. Tonbul, S. Akbayrak, S. Özkaz, *Int. J. Hydrogen Energy* **2016**, *41*, 11154-11162.
- [16] a) Y.-Z. Chen, R. Zhang, L. Jiao, H.-L. Jiang, *Coord. Chem. Rev.* **2018**, *362*, 1-23; b) R. J. White, R. Luque, V. L. Budarin, J. H. Clark, D. J. Macquarrie, *Chem. Soc. Rev.* **2009**, *38*, 481-494.
- [17] J. Feng, Y. He, Y. Liu, Y. Du, D. Li, *Chem. Soc. Rev.* **2015**, *44*, 5291-5319.
- [18] G. Fan, F. Li, D. G. Evans, X. Duan, *Chem. Soc. Rev.* **2014**, *43*, 7040-7066.
- [19] a) X. Sun, G. Wang, H. Sun, F. Lu, M. Yu, J. Lian, *J. Power Sources* **2013**, *238*, 150-156; b) B. Han, G. Cheng, E. Y. Zhang, L. J. Zhang, X. K. Wang, *Electrochim. Acta* **2018**, *263*, 391-399.
- [20] P. He, X.-Y. Yu, X. W. Lou, *Angew. Chem. Int. Ed.* **2017**, *56*, 3897-3900.
- [21] D. Xia, H. Chen, J. Jiang, L. Zhang, Y. Zhao, D. Guo, J. Yu, *Electrochim. Acta* **2015**, *156*, 108-114.
- [22] C. Xing, F. Musharavati, H. Li, E. Zalezhad, O. K. S. Hui, S. Bae, B.-Y. Cho, *RSC Adv.* **2017**, *7*, 38945-38950.
- [23] Z. Li, T. He, L. Liu, W. Chen, M. Zhang, G. Wu, P. Chen, *Chem. Sci.* **2017**, *8*, 781-788.
- [24] Z.-C. Fu, Y. Xu, S. L.-F. Chan, W.-W. Wang, F. Li, F. Liang, Y. Chen, Z.-S. Lin, W.-F. Fu, C.-M. Che, *Chem. Commun.* **2017**, *53*, 705-708.
- [25] S.-K. Park, J. K. Kim, Y. C. Kang, *Chem. Eng. J.* **2017**, *328*, 546-555.
- [26] Z. Jiang, Z. Li, Z. Qin, H. Sun, X. Jiao, D. Chen, *Nanoscale* **2013**, *5*, 11770-11775.

COMMUNICATION

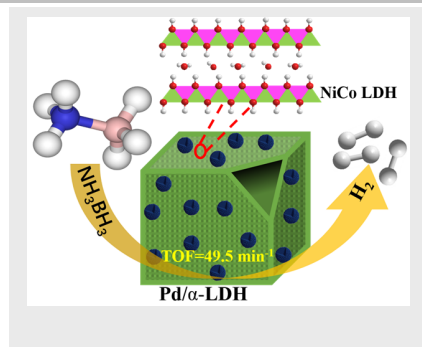
- [27] H. Hu, B. Guan, B. Xia, X. W. Lou, *J. Am. Chem. Soc.* **2015**, *137*, 5590-5595.
- [28] Y. Wang, S. Gai, C. Li, F. He, M. Zhang, Y. Yan, P. Yang, *Electrochim. Acta* **2013**, *90*, 673-681.
- [29] Q. Zhang, J. Xu, D. Yan, S. Li, J. Lu, X. Cao, B. Wang, *Catal. Sci. Technol.* **2013**, *3*, 2016.
- [30] W. Liu, J. Bao, M. Guan, Y. Zhao, J. Lian, J. Qiu, L. Xu, Y. Huang, J. Qian, H. Li, *Dalton Trans* **2017**, *46*, 8372-8376.
- [31] J. Zhao, M. Shao, D. Yan, S. Zhang, Z. Lu, Z. Li, X. Cao, B. Wang, M. Wei, D. G. Evans, X. Duan, *J. Mater. Chem. A* **2013**, *1*, 5840.
- [32] B. Kılıç, S. Şencanlı, Ö. Metin, *J. Mol. Catal. A: Chem.* **2012**, *361-362*, 104-110.
- [33] Q. Wang, Z. Liu, W. Wang, D. Liu, W. Shi, J. He, P. Shao, R. Shi, F. Cui, *Int. J. Hydrogen Energy* **2016**, *41*, 8470-8478.
- [34] Ö. Metin, E. Kayhan, S. Özkar, J. J. Schneider, *Int. J. Hydrogen Energy* **2012**, *37*, 8161-8169.
- [35] W.-D. Zhong, X.-K. Tian, C. Yang, Z.-X. Zhou, X.-W. Liu, Y. Li, *Int. J. Hydrogen Energy* **2016**, *41*, 15225-15235.
- [36] W. Wang, Z.-H. Lu, Y. Luo, A. Zou, Q. Yao, X. Chen, *ChemCatChem* **2018**, doi.org/10.1002/cctc.201701989.
- [37] Y. Liu, H. Guan, J. Zhang, Y. Zhao, J.-H. Yang, B. Zhang, *Int. J. Hydrogen Energy* **2018**, *43*, 2754-2762.
- [38] J. Wang, Y. L. Qin, X. Liu, X. B. Zhang, *J. Mater. Chem.* **2012**, *22*, 12468-12470.
- [39] J. Manna, S. Akbayrak, S. Özkar, *RSC Adv.* **2016**, *6*, 102035-102042.
- [40] C. Wang, J. Tuninetti, Z. Wang, C. Zhang, R. Ciganda, L. Salmon, S. Moya, J. Ruiz, D. Astruc, *J. Am. Chem. Soc.* **2017**, *139*, 11610-11615.
- [41] a) Z. Zhang, Z.-H. Lu, H. Tan, X. Chen, Q. Yao, *J. Mater. Chem. A* **2015**, *3*, 23520-23529; b) C. Y. Peng, L. Kang, S. Cao, Y. Chen, Z. S. Lin, W. F. Fu, *Angew. Chem. Int. Ed.* **2015**, *54*, 15725-15729.
- [42] Y.-H. Zhou, S. Wang, Y. Wan, J. Liang, Y. Chen, S. Luo, C. Yong, *J. Alloys Compd.* **2017**, *728*, 902-909.
- [43] D. Sun, V. Mazumder, Ö. Metin, S. Sun, *ACS Nano* **2011**, *5*, 6458-6464.

COMMUNICATION

Entry for the Table of Contents

COMMUNICATION

Pd nanoparticles (NPs) were highly dispersed onto the hollow NiCo layered double hydroxide (LDH) derived from ZIF-67, through the *in situ* reduction method. The nanocomposite exhibited the superior catalytic performance for hydrogen generation from ammonia borane in aqueous solution at room temperature.



Author(s), Corresponding Author(s)*
Ying-Hua Zhou,* Suqin Wang, Zhiyan
Zhang, Nicholas Williams, Yong Cheng
and Jing Gu*

Page No. – Page No.

Hollow NiCo Layered Double
Hydroxide Supported Pd Catalysts for
Superior Hydrogen Evolution Activity
for Hydrolysis of Ammonia Borane